



Nanoscale

ARTICLE

Higher order Fano graphene metamaterials for nanoscale optical sensing[†]

Received 00th January 20xx,

Xiangdong Guo,^{a,b,c} Hai Hu,^{a,c} Xing Zhu,^{a,b,d} Xiaoxia Yang,^{*a} Qing Dai^{*a}

Accepted 00th January 20xx

DOI: 10.1039/x0xx00000x

www.rsc.org/

Plasmonic Fano metamaterials provide a unique platform for optical sensing applications due to their sharp spectral response and ability to confine light to nanoscale regions that make them strong prospect for refractive-index sensing. Higher order Fano resonance modes in noble metal plasmonic structures can further improve the sensitivity, but their applications are heavily limited by crosstalk between different modes due to the large damping rates and broadband spectral responses of the metal plasmon modes. Here, we create pure higher order Fano modes by designing asymmetric metamaterials comprised of a split-ring resonator and disk with the low-loss graphene plasmon. These higher order modes are highly sensitive to nanoscale analyte (8 nm thick) both in refractive-index and infrared vibrational fingerprints sensing, as demonstrated by the numerical calculation. The frequency sensitivity and figure-of-merit of hexacontatetrapolar mode can reach 289 cm⁻¹/RIU and 29, respectively, and it can probe the weak infrared vibrational modes of the analyte with more than 400 times enhancement. The enhanced sensitivity and tunability of higher order Fano graphene metamaterials promise a high-performance nanoscale optical sensor.

Introduction

Fano resonance with spectrally narrow optical responses and high local field enhancement has been demonstrated in plasmonic metamaterials,¹⁻³ which has allowed them to emerge as a powerful photonic platform for sensing applications.⁴⁻⁹ Plasmonic Fano structures can detect small amounts of molecules by measuring frequency shifts of the narrow optical response induced by a refractive index change of the local environment.^{1, 5, 6, 9} Based on this application, many noble metal Fano structures have been designed, such as ring/disk cavity,^{4, 10, 11} "X" shape structure¹² and many other. Plasmonic Fano resonances are the coupling of the bright plasmon mode (broad) and dark plasmon modes (narrow). The dipolar (D) plasmon is often the bright mode, which can be directly excited by normally incident light. In contrast, the higher order (quadrupolar (Q), octupolar (O), hexadecapolar (H), triakontadipolar (T), etc.) plasmons are usually the dark mode, which are hard to be optically excited.

In order to enhance the sensitivity of the refractive-index sensor, the plasmon resonance should satisfy basic characteristics: a high spectral shift $\delta\lambda/\delta n$ (refractive index) and a narrow line width.¹² The

higher order plasmons have the sharper peaks with higher quality factors.¹³ In Fano structures, the higher order modes would be exhibited and the same refractive index change could induce larger frequency shifts with mode order increases. Thus the higher order Fano resonances have greater sensitivity in refractive-index sensing^{6, 9, 14}. However, in the noble metal systems, many adjacent higher order modes can potentially exist crosstalk,^{9, 14} which originates from the large plasmonic damping rates and broad-band spectral responses of the bright mode. For example, different higher order Fano modes interact with each other in the gold ring/disk cavity, where the disk's dipolar plasmon acts as a bright mode and the ring's multipolar plasmons act as dark modes. To overcome this problem and to realize high-quality higher-order Fano resonance for ultra-sensitive refractive index sensing, graphene plasmons with low damping rates¹⁵⁻¹⁷ and high field confinement could be used.

In addition to sensitive refractive-index sensing, graphene plasmons in the infrared frequency range can also be used for surface-enhanced infrared absorption (SEIRA)¹⁸⁻²⁰. SEIRA, which can directly provide chemical information about analytes by characterizing their molecular fingerprints, is complementary to refractive index sensors.²¹ The high local field enhancement in plasmonic Fano structures means the high sensitivity of SEIRA. Moreover, Fano resonance creates two resonant absorption peaks with wide spectral ranges, which can enhance multiple vibration signals of molecules at a given time. Thus, it provides a platform for multispectral biosensing.²

In this manuscript, the low damping graphene plasmon is used to generate separate higher order Fano modes for enhanced refraction-index sensing and SEIRA. We adapt a commonly used hybrid structure of a split-ring resonator (SRR) and disk,²²⁻²⁴ where

^a China CAS Center for Excellence in Nanoscience, National Center for Nanoscience and Technology, Beijing 100190, P. R. China.

E-mail: daig@nanoctr.cn, yangqx@nanoctr.cn; Tel: +86-010-82545720

^b Academy for Advanced Interdisciplinary Studies, Peking University, Beijing 100871, P. R. China.

^c University of Chinese Academy of Sciences, Beijing 100049, P. R. China.

^d State Key Lab for Mesoscopic Physics, School of Physics, Peking University, Beijing 100871, P. R. China.

[†] Electronic Supplementary Information (ESI) available: [details of any supplementary information available should be included here]. See DOI: 10.1039/x0xx00000x

Nanoscale

ARTICLE

the higher order plasmon resonance excited in the SRR act as dark mode and the dipolar plasmon resonance of the graphene disk acts as bright mode. Each higher order Fano resonance, i.e. H, T, and hexacatetrapolar (HC) Fano, can be realized by choosing proper size of the graphene disk. As the mode order increases, its sensitivity to the refractive index change increases. The sensitivity

of the HC Fano mode reaches $289 \text{ cm}^{-1}/\text{RIU}$, corresponding to a FOM of 29 for the refractive-index sensor. Moreover, the highly confined electromagnetic field of these higher order Fano resonances can also be used to enhance the molecular vibrational modes.

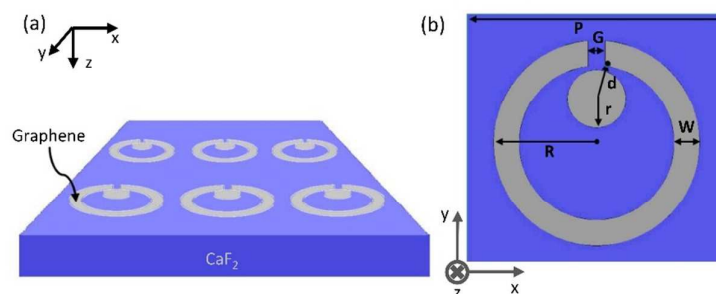


Fig. 1 (a) Schematic of the graphene metamaterial comprised of a disk and a SRR in a unit cell. (b) Top view of a unit cell: fixed periodicity $P = 300 \text{ nm}$, outer radius $R = 120 \text{ nm}$, width $W = 30 \text{ nm}$, and gap $G = 20 \text{ nm}$ of the graphene SRR, and the closest separation distance $g = d - r$ of graphene disk and SRR.

Results and discussion

Structural design and physical mechanism

A schematic of the graphene metamaterials for higher order Fano resonance is shown in Fig. 1. They are comprised of a graphene disk positioned inside of a graphene SRR in a unit cell. The unit cells are arranged in a square lattice. The 300 nm CaF_2 film is chosen as substrate over the commonly used substrates like SiO_2 and $h\text{-BN}$,^{16, 25} since CaF_2 is transparent and has no phonon that can interact with graphene plasmon in the infrared spectral region.^{18, 26, 27} The proposed Fano resonance is excited by a plane wave propagating in the z -direction with an electric field polarized in the x -direction.

The higher order Fano resonances of the graphene metamaterials are simulated employing the finite element method (FEM). Graphene is modeled as a material with finite thickness and equivalent relative permittivity, which is thickness dependent. The equivalent relative permittivity is derived from the surface conductivity. It is calculated

by $\varepsilon_g = i\sigma / \varepsilon_0\omega t_g$,²⁸ where ε_0 is the permittivity of free space and the graphene layer thickness is $t_g = 1 \text{ nm}$, at which the calculations reach proper convergence. Thus the graphene layer is treated as the transition boundary condition. The permittivity of CaF_2 is obtained from the handbook.²⁹ To balance the 3D FEM calculated amount and the mesh quality, the smallest mesh size of graphene is 0.5 nm and the mesh size gradually increases outside the graphene layer.

To calculate the surface conductivity of graphene, σ , the Kubo formula³⁰⁻³³ is used, which consists of interband and intraband

transitions. At room temperature ($T = 300 \text{ K}$), which satisfies the requirement of $K_B T \ll E_f$, the expression is approximated as:

$$\sigma = \frac{ie^2 E_f}{\pi \hbar^2 (\omega + i\tau^{-1})} + \frac{ie^2}{4\pi \hbar} \ln \left[\frac{2|E_f| - \hbar(\omega + i\tau^{-1})}{2|E_f| + \hbar(\omega + i\tau^{-1})} \right] \quad (1)$$

In this equation, the first term corresponds to the intraband transition, and the second term corresponds to the direct interband transition. The angular frequency is $\omega = 2\pi\nu$, e is electron charge, \hbar is the reduced Planck constant, and E_f is the doped graphene Fermi energy. The relaxation time $\tau = \mu E_f / ev_f^2$, where $v_f = c/300$ is the Fermi velocity and $\mu = 10000 \text{ cm}^2 \text{V}^{-1} \text{s}^{-1}$ is the carrier mobility of graphene.

Generating higher order Fano Resonance modes

Here, we take a SRR structure with outer radius $R = 120 \text{ nm}$, the gap $G = 20 \text{ nm}$, width $W = 30 \text{ nm}$ and periodic lattice parameter $P = 300 \text{ nm}$ as an example to illustrate the as-proposed higher order Fano resonance in the mid-infrared range. This dimension can ensure the excitation energies lower than the energy of graphene's intrinsic optical phonons (a type of lattice vibration) at $1,580 \text{ cm}^{-1}$. Thus the graphene SRR is far away from Landau damping region and has low damping rate.^{15, 34} The transmission spectrum of the SRR exhibits six absorption peaks at $467, 550, 756, 964, 1146$ and 1309 cm^{-1} in the range studied (black curve in Fig. 2a). The calculated method of transmission spectrum is in the ESI†. The SRR structure derives from the break of symmetry of a graphene ring with a 20 nm gap. For comparison, the transmission spectrum of the corresponding graphene ring without a slit is also plotted (red curve in Fig. 2a). The

Nanoscale

ARTICLE

spectrum has only one peak, which is at 467 cm^{-1} . To understand the transmission spectra, the z-complement electric near field of the ring and SRR at corresponding resonant frequencies are displayed in Fig. 2b. The electromagnetic field distribution indicates a dipolar oscillation mode in the ring. However, due to the broken symmetry,³⁵⁻³⁷ there are 4, 6, 8, 10, and 12 nodes in the electromagnetic field distribution of the SRR, corresponding to Q, O, H, T, and HC dark modes, respectively.^{37,38} The relation between the node number, m , and the order number of the mode, n , is $m=2n$. Thus, the 2^{nd} order electromagnetic resonance is produced.

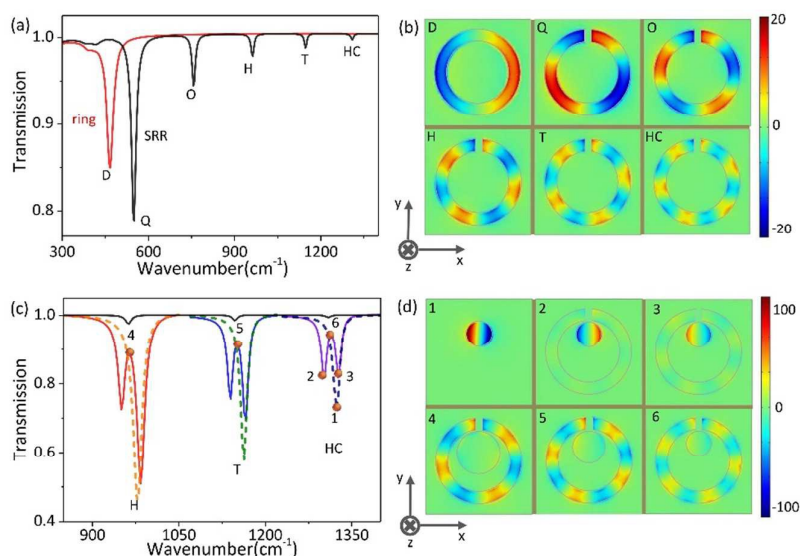
The radius of the graphene disk r is then designed to overlap with the higher order plasmon frequency of the SRR in the following. The as-excited plasmons in the graphene disks are the dipolar electromagnetic resonance, as demonstrated by the calculated electric near field distribution in Fig. 2d (1). Their plasmon frequency varies with the disk radius r according to the equation³⁹⁻⁴²

$$\omega_{pl} = \sqrt{\frac{e^2 E_f q}{2\pi \hbar^2 \epsilon_0 \epsilon_r}} \propto \sqrt{\frac{E_f}{r \epsilon_r}} \quad (2)$$

Where $q = \pi/2r$ is the wave vector and ϵ_r is determined by the dielectric environment. Thus, the disk size can be manipulated to adjust the plasmon frequency to match a higher order resonance mode in the SRR. Such as shown in Fig. 2c, transmission spectra of graphene disks with radii of 60, 43.5 and 34 nm have resonance frequencies at 979, 1163 and 1323 cm^{-1} , respectively, which correspond to the H, T, and HC modes of the graphene SRR.

Higher order Fano resonances are generated by inserting a disk into the SRR. The higher order Fano resonance, i.e. the H, T, and HC Fano mode, occurs when the dipolar plasmon frequency covers the corresponding higher order mode of the SRR (Fig. 2c). The dipolar mode in the disk is the bright mode (large resonance peak), while the higher order SRR modes are dark (small peaks). This is consistent with the near electric field distributions of the SRR (i.e. weak Q-HC modes in Fig. 2b) and the disk (strong mode in Fig. 2d). Here, the closest separation g between the disk and the gap is chosen as 5 nm ,⁴³ but when g increases to 15 nm , these modes can still interact with each other well to form the higher order Fano modes (details can be found in the Fig. S2 in the ESI†).

To study the physical mechanism of the higher order Fano resonance, the near field distribution in the SRR-disk hybrid structure is analyzed. Take the HC mode as an example. Its near field distribution at two resonance peaks and the transparency window (points 2, 3, and 6 in Fig. 2c) are displayed in Fig. 2d. At point 6, where the strongest destructive coupling happens, the electromagnetic energy of the disk almost completely transfers to the SRR, whose near electric field enhancement is one order of magnitude larger than the SRR alone (Fig. 2b). At points 2 and 3, most of the electromagnetic energy remains in the disk, and the near field strength of the SRR is almost equivalent to that in an individual SRR, indicating a weak-coupling strength between the disk and the SRR. The near field distribution of the H and T Fano modes at the strongest coupling points (points 4 and 5), shown in Fig. 2d, also demonstrate a strong energy transfer between the SRR and disk.



Nanoscale

ARTICLE

Fig. 2 (a) Transmission spectra of ring array (red) and SRR array (black). (b) Electric near field distributions (the z-component, normalized to the incident light) of the ring and SRR unit cell of different modes. (c) The transmission spectra of the Fano metamaterials with H, T, and HC order modes (colored solid lines), respectively. The transmission spectra of the individual disk array (dashed lines) and SRR array (black) are also plotted. (d) Normalized z-component electric near field distributions of different modes at frequencies: (1) 1323 cm^{-1} , (2) 1304 cm^{-1} , (3) 1327 cm^{-1} , (4) 963 cm^{-1} , (5) 1150 cm^{-1} and (6) 1314 cm^{-1} , as marked with orange dots in (c). The cutting plane is 2 nm above the bottom of graphene metamaterials. Graphene E_f is 0.5 eV.

Refractive-index sensing performance of the higher order Fano resonance

We now proceed to evaluate the performance of these separate higher order Fano modes. An 8 nm thick film with different refractive indices is applied over the device as an analyte. Fig. 3a shows the transmission spectra of the HC Fano resonance modes with several typical analytes, i.e., $n=1$ (air), $n \approx 1.32$ (Ethanol), $n \approx 1.41$ (Ethylene glycol), and $n \approx 1.56$ (Bromoform). Here, the E_f is fixed at 0.5 eV. The transparency window frequency shifts to red (from 1314 cm^{-1} to 1152 cm^{-1}) as the refractive index of the analytes increase from 1 to 1.56. The transparency window frequencies of the H, T, and HC Fano modes are plotted together as a function of the refractive index (Fig. 3b). There is a linear change in these frequency shifts, and the slopes of these lines are defined as the sensitivity (approximately 195, 239, and 289 $\text{cm}^{-1}/\text{RIU}$ for the H, T, and HC Fano modes, respectively). This clearly reflects that the sensitivity of the sensor is enhanced by the graphene higher order Fano resonance.

The ratio of the sensitivity to the bandwidth of the resonance [$(\text{cm}^{-1}/\text{RIU})/\text{bandwidth}$] determines the FOM of metamaterials. The bandwidth is the full width at half-maximum (FWHM) in the symmetric Fano resonance. In the asymmetric Fano resonance, the bandwidth is the line width from the peak to the dip of the

resonance⁹. The FOM values of the H, T, and HC Fano are around 15, 24, and 29, respectively. It not only reveals the FOM is on the rise when increasing order number n of the Fano resonance, but also indicates the maximum FOM in our structures comes from the HC Fano. To understand this result, the wave vector k_{spp} of the higher order plasmon modes in the SRR satisfy the equations $k_{\text{spp}} \propto n/L$ ⁴⁴⁻⁴⁷ and $k_{\text{spp}} = \hbar\omega_r^2 / (2\alpha_0 E_f c)$ ^{48, 49}, where n is the order of the mode, L is the length of the SRR, and $\alpha_0 = e^2 / \hbar c$ is the fine-structure constant. Thus, the frequency of the transparency windows in higher order Fano satisfy the equation $\omega_r \propto \sqrt{nE_f/L} \propto \sqrt{1/(L/n)}$, where L/n is regarded as the effective resonance length of the graphene dipolar plasmon. When the order number n of the Fano resonance is larger, the effective resonance length is shorter. Thus, the frequency shift is faster, and the sensitivity is improved. In addition, the higher order Fano resonance has the narrower FWHM, which decreases from 13 to 9.9 cm^{-1} corresponding to ranging from H to HC Fano resonance. Hence, the sensitivity and FOM are enhanced with increasing order number n of the Fano resonance.

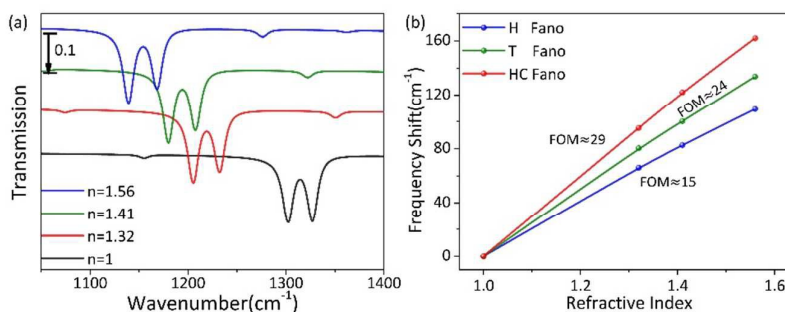


Fig. 3 (a) Simulated transmission spectra of the HC Fano resonance mode with different analytes (marked by refractive indices). (b) Frequency shift of H, T, and HC Fano resonance modes versus the refractive index of the analyte. The corresponding FOM values are also shown.

Dynamic tunability and the SEIRA applications of the higher order Fano resonance modes

The ability to tune graphene higher order Fano resonances stemming from its tunable Fermi level is significant for dynamic biosensors. For example, the transparency windows in the transmission spectra of the HC mode increase in resonant strength and shift to blue as E_f is adjusted from 0.4 to 0.6 eV (Fig. 4a), which can be realized by chemical doping via nitric acid vapor or NO_2 .^{15, 50}

This phenomenon can be interpreted in the following. The resonant frequency of the SRR increases with E_f via $\omega_r \propto \sqrt{nE_f/L}$. And the graphene disk plasmon frequency also increases with E_f (equation 2). Thus, the resulting

higher order Fano resonant frequencies can be tuned by changing the E_f while fixing the structure parameter. We plot the resonant

Nanoscale

ARTICLE

frequency shifts of the transparency window of the H, T, and HC Fano modes as a function of $E_f^{1/2}$ in Fig. 4b. The higher order the mode is, then the faster the frequency shift. Thus, the sensitivity is

expressed by the equation $\partial\omega_r/\partial E_f \propto \sqrt{n}/LE_f^{-1/2}$. When E_f is fixed, a larger n results in greater sensitivity.

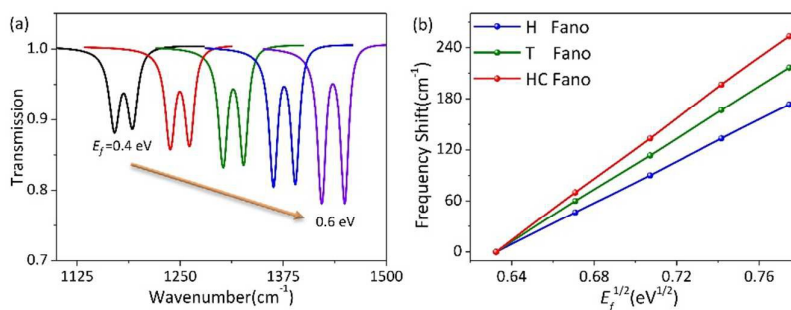
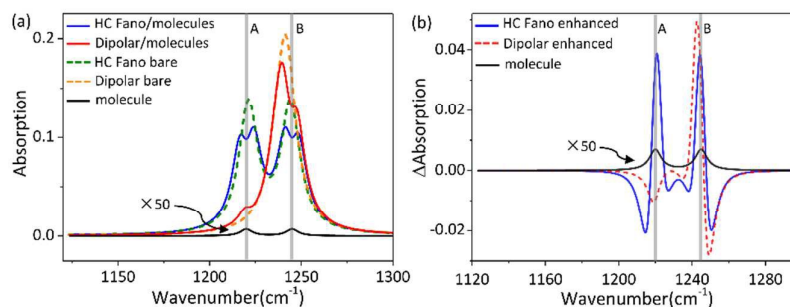


Fig. 4 (a) Simulated transmission spectra of the HC Fano resonance structure with E_f varied from 0.4 eV to 0.6 eV. (b) The peak frequency in transparency window of H, T, and HC Fano resonance modes in the transmission spectra as a function of $E_f^{1/2}$

The dynamical tunable graphene plasmon higher order Fano resonance with high electromagnetic field confinement in the mid-infrared range supplies a very promising route to identify molecules via SEIRA. SEIRA is complementary to refractive index sensors since it can detect molecular vibrational fingerprints. The Fano resonance exhibits multiple resonant absorption peaks which can reduce the detuning between the plasmon resonant frequency and multiple vibrational frequencies and can be used as a platform for enhancing multiple vibrational modes of molecules. The HC Fano mode of the asymmetric structure and the dipolar mode of the disk are comparatively studied for SEIRA application. An 8-nm-thick tert-Butylamine ($(\text{CH}_3)_3\text{CNH}_2$) layer is used as the analyte which has two vibrational modes at $\sim 1220 \text{ cm}^{-1}$ (A) and $\sim 1245 \text{ cm}^{-1}$ (B) corresponding to the C-C-C symmetric and anti-symmetric stretches, respectively. An analytical model based on summing Lorentz oscillators⁵¹⁻⁵³ is used to simulate the molecule's vibrational spectrum (Fig. 5a) as follows:

$$\varepsilon(\omega) = 1 + \sum_{n=1}^N \frac{f_n}{\omega_n^2 - \omega^2 - i\gamma_n\omega} \quad (3)$$



Where f_n , ω_n and γ_n are parameters characterizing individual vibrations, i.e. ($f_1=f_2=215 \text{ cm}^{-2}$, $\gamma_1=\gamma_2=50 \text{ cm}^{-1}$, $\omega_1=1220 \text{ cm}^{-1}$, $\omega_2=1245 \text{ cm}^{-1}$). The direct IR absorption of the 8-nm-thick tert-Butylamine layer is very weak (0.014%) at A and B, which is undetectable in the commercial FTIR¹⁸. The graphene E_f is adjusted to 0.437 eV to realize the spectral overlap between the molecules and graphene metamaterials. After the enhancement of the graphene metamaterials, the A and B modes are present as obvious dips in the plasmon resonant absorption spectra (solid lines). As shown, the HC Fano mode has two prominent resonance peaks exactly at the molecular modes (green dashed line) and significantly enhances the signals of both A and B modes. As a comparison, the dipolar plasmon mode (supported graphene disk) only has one resonance peak (orange dashed line). The A vibrational frequency is out of range for the plasmon resonant frequency and the enhanced vibrational signal is much weaker than the B vibrational mode.

Nanoscale

ARTICLE

Fig. 5 (a) Absorption spectra of graphene HC Fano modes and corresponding graphene disk before (dashed lines) and after (solid lines) analyte layer coating with E_f of 0.437 eV. The absorption spectrum of the 8-nm-thick tert-Butylamine is also plotted (black curve), with two vibrational modes A and B. (b) The molecular vibrational mode response in plasmon resonant peaks extracted from (a).

The difference between absorption spectra, i.e. the delta absorption, before and after coating with the tert-Butylamine film applied are extracted to calculate the enhancement of IR signals of the vibrational modes. The delta absorption of the HC modes are displayed in Fig. 5b. The enhancement factors of both the A and B modes are up to 425-fold from the HC order Fano modes. However, the enhancement factor of the A mode is only 75, about 7.5 times smaller than that of the B modes (enhanced 554-fold).

Conclusions

In summary, the pure high-quality higher order Fano resonances have been demonstrated in graphene plasmonic metamaterials. The crosstalk between different higher order Fano modes is avoided due to the narrow bandwidth of the graphene plasmon resulted from its low damping. The higher order Fano modes have superior refractive-index sensing performance because the spectral shifts induced by analyte increase with Fano mode order. In this work, the frequency sensitivity and FOM of the HC mode are able to reach $289 \text{ cm}^{-1}/\text{RIU}$ and 29 for 8 nm thick analyte. Moreover, these graphene Fano modes can also be tuned to probe the infrared vibrational fingerprints of the analyte with a significant signal enhancement (>400 times). Therefore, our proposed higher order Fano structures are a promising method for nanoscale optical sensing.

Acknowledgements

This work was supported by The National Basic Research Program of China (Grant No. 2015CB932400, 2016YFA0201600), the National Natural Science Foundation of China (Grant No. 51372045, 11504063, 11674073), the Bureau of International Cooperation, Chinese Academy of Sciences (121D11KYSB20130013), and the key program of the Bureau of Frontier Sciences and Education Chinese Academy of Sciences (QYZDB-SSW-SLH021).

Notes and references

- B. Luk'yanchuk, N. I. Zheludev, S. A. Maier, N. J. Halas, P. Nordlander, H. Giessen and C. T. Chong, *Nature materials*, 2010, **9**, 707-715.
- C. Wu, A. B. Khanikaev, R. Adato, N. Arju, A. A. Yanik, H. Altug and G. Shvets, *Nature materials*, 2011, **11**, 69-75.
- N. Verellen, Y. Sonnefraud, H. Sobhani, F. Hao, V. V. Moshchalkov, P. V. Dorpe, P. Nordlander and S. A. Maier, *Nano letters*, 2009, **9**, 1663-1667.
- Y. Zhang, T. Li, B. Zeng, H. Zhang, H. Lv, X. Huang, W. Zhang and A. K. Azad, *Nanoscale*, 2015, **7**, 12682-12688.
- N. Liu, T. Weiss, M. Mesch, L. Langguth, U. Eigenthaler, M. Hirscher, C. Sonnichsen and H. Giessen, *Nano letters*, 2010, **10**, 1103-1107.
- W. Tang, L. Wang, X. Chen, C. Liu, A. Yu and W. Lu, *Nanoscale*, 2016, **8**, 15196-15204.
- F. Hao, P. Nordlander, Y. Sonnefraud, P. V. Dorpe and S. A. Maier, *ACS nano*, 2009, **3**, 643-652.
- M. Amin, M. Farhat and H. Bagci, *Scientific reports*, 2013, **3**, 2105.
- Y. H. Fu, J. B. Zhang, Y. F. Yu and B. Luk'yanchuk, *ACS nano*, 2012, **6**, 5130-5137.
- Y. Sonnefraud, N. Verellen, H. Sobhani, G. A. Vandenbosch, V. V. Moshchalkov, P. Van Dorpe, P. Nordlander and S. A. Maier, *ACS nano*, 2010, **4**, 1664-1670.
- Q. Zhang, X. Wen, G. Li, Q. Ruan, J. Wang and Q. Xiong, *ACS Nano*, 2013, **7**, 11071-11078.
- N. Verellen, P. Van Dorpe, C. Huang, K. Lodewijks, G. A. Vandenbosch, L. Lagae and V. V. Moshchalkov, *Nano letters*, 2011, **11**, 391-397.
- H. Liu, Z. Wang, J. Huang, Y. J. Liu, H. J. Fan, N. I. Zheludev and C. Soci, *Nano letters*, 2014, **14**, 5162-5169.
- Y. Zhang, T. Jia, H. Zhang and Z. Xu, *Optics letters*, 2012, **37**, 4919-4921.
- H. Yan, T. Low, W. Zhu, Y. Wu, M. Freitag, X. Li, F. Guinea, P. Avouris and F. Xia, *Nature Photonics*, 2013, **7**, 394-399.
- X. Yang, F. Zhai, H. Hu, D. Hu, R. Liu, S. Zhang, M. Sun, Z. Sun, J. Chen and Q. Dai, *Advanced materials*, 2016, **28**, 2931-2938.
- J. Christensen, A. Manjavacas, S. Thongrattanasiri, F. H. Koppens and F. J. Garcia de Abajo, *ACS nano*, 2011, **6**, 431-440.
- H. Hu, X. Yang, F. Zhai, D. Hu, R. Liu, K. Liu, Z. Sun and Q. Dai, *Nature communications*, 2016, **7**, 12334.
- D. Rodrigo, O. Limaj, D. Janner, D. Etezadi, F. J. G. de Abajo, V. Pruneri and H. Altug, *Science*, 2015, **349**, 165-168.
- R. Adato, A. A. Yanik, J. J. Amsden, D. L. Kaplan, F. G. Omenetto, M. K. Hong, S. Erramilli and H. Altug, *Proceedings of the National Academy of Sciences of the United States of America*, 2009, **106**, 19227-19232.
- I. M. Pryce, Y. A. Kelaita, K. Aydin and H. A. Atwater, *ACS nano*, 2011, **5**, 8167-8174.
- N. Liu, L. Langguth, T. Weiss, J. Kastel, M. Fleischhauer, T. Pfau and H. Giessen, *Nature materials*, 2009, **8**, 758-762.
- S. Zhang, D. A. Genov, Y. Wang, M. Liu and X. Zhang, *Physical review letters*, 2008, **101**, 047401.
- X. Zhao, C. Yuan, L. Zhu and J. Yao, *Nanoscale*, 2016, **8**, 15273-15280.
- V. W. Brar, M. S. Jang, M. Sherrott, J. J. Lopez and H. A. Atwater, *Nano letters*, 2013, **13**, 2541-2547.
- M. Abb, Y. Wang, N. Papisimakis, C. De Groot and O. L. Muskens, *Nano letters*, 2013, **14**, 346-352.
- M. Abb, Y. Wang, N. Papisimakis, C. H. de Groot and O. L. Muskens, *Nano letters*, 2014, **14**, 346-352.
- X. T. Kong, X. Yang, Z. Li, Q. Dai and X. Qiu, *Optics letters*, 2014, **39**, 1345-1348.
- E.D. Palik, Handbook of optical constants of solids, *Academic Press*, London, 1985.
- P.-Y. Chen and A. Alù, *ACS nano*, 2011, **5**, 5855-5863.

Nanoscale

ARTICLE

31. L. A. Falkovsky and S. S. Pershoguba, *Physical Review B*, 2007, **76**.
32. B. Vasić, M. M. Jakovljević, G. Isić and R. Gajić, *Applied Physics Letters*, 2013, **103**, 011102.
33. V. P. Gusynin, S. G. Sharapov and J. P. Carbotte, *Journal of Physics: Condensed Matter*, 2007, **19**, 026222.
34. H. Buljan, M. Jablan and M. Soljačić, *Nature Photonics*, 2013, **7**, 346-348.
35. F. Hao, E. M. Larsson, T. A. Ali, D. S. Sutherland and P. Nordlander, *Chemical Physics Letters*, 2008, **458**, 262-266.
36. H. Wang, Y. Wu, B. Lassiter, C. L. Nehl, J. H. Hafner, P. Nordlander and N. J. Halas, *Proceedings of the National Academy of Sciences of the United States of America*, 2006, **103**, 10856-10860.
37. A. K. Sheridan, A. W. Clark, A. Glidle, J. M. Cooper and D. R. S. Cumming, *Applied Physics Letters*, 2007, **90**, 143105.
38. C. Rockstuhl, F. Lederer, C. Etrich, T. Zentgraf, J. Kuhl and H. Giessen, *Optics express*, 2006, **14**, 8827-8836.
39. H. Hu, F. Zhai, D. Hu, Z. Li, B. Bai, X. Yang and Q. Dai, *Nanoscale*, 2015, **7**, 19493-19500.
40. S. H. Abedinpour, G. Vignale, A. Principi, M. Polini, W.-K. Tse and A. H. MacDonald, *Physical Review B*, 2011, **84**.
41. A. N. Grigorenko, M. Polini and K. S. Novoselov, *Nature Photonics*, 2012, **6**, 749-758.
42. R. Liu, B. Liao, X. Guo, D. Hu, H. Hu, L. Du, H. Yu, G. Zhang, X. Yang and Q. Dai, *Nanoscale*, 2017, **9**, 208-215.
43. X.-j. Shang, X. Zhai, X.-f. Li, L.-l. Wang, B.-x. Wang and G.-d. Liu, *Plasmonics*, 2016, **11**, 419-423.
44. X. Shi, D. Han, Y. Dai, Z. Yu, Y. Sun, H. Chen, X. Liu and J. Zi, *Opt Express*, 2013, **21**, 28438-28443.
45. S. Liu, Z. Zhang and Q. Wang, *Optics express*, 2009, **17**, 2906-2917.
46. P. Nordlander, *ACS Nano*, 2009, **3**, 488-492.
47. P. Liu, W. Cai, L. Wang, X. Zhang and J. Xu, *Applied Physics Letters*, 2012, **100**, 153111.
48. H. Cheng, S. Chen, P. Yu, X. Duan, B. Xie and J. Tian, *Applied Physics Letters*, 2013, **103**, 203112.
49. F. H. Koppens, D. E. Chang and F. J. Garcia de Abajo, *Nano letters*, 2011, **11**, 3370-3377.
50. A. L. Falk, K. C. Chiu, D. B. Farmer, Q. Cao, J. Tersoff, Y. H. Lee, P. Avouris and S. J. Han, *Physical review letters*, 2017, **118**, 257401.
51. F. Liu and E. Cubukcu, *Physical Review B*, 2013, **88**, 115439.
52. A. Marini, I. Silveiro and F. J. Garcia de Abajo, *ACS Photonics*, 2015, **2**, 876-882.
53. E. Cubukcu, S. Zhang, Y.-S. Park, G. Bartal and X. Zhang, *Applied Physics Letters*, 2009, **95**, 043113.